Probing equilibrium glass flow up to exapoise viscosities

Eva Arianna Aurelia Pogna[a], Cristian Rodríguez-Tinoco[b], Giulio Cerullo[c], Carino Ferrante[a], Javier Rodríguez-Viejo[b,d], and Tullio Scopigno[a,1]

[a]Dipartimento di Fisica, Universitá di Roma "La Sapienza," I-00185, Rome, Italy; [b]Nanomaterials and Microsystems Group, Physics Department, Universitat Autònoma de Barcelona, ES-08193, Bellaterra, Spain; [c]Istituto di Fotonica e Nanotecnologie-CNR, Dipartimento di Fisica, Politecnico di Milano, I-20133, Milan, Italy; and [d]MATGAS 2000 AIE, Universitat Autònoma de Barcelona, E-08193, Bellaterra, Spain

Edited by David A. Weitz, Harvard University, Cambridge, MA, and approved January 15, 2015 (received for review December 9, 2014)

Glasses are out-of-equilibrium systems aging under the crystallization threat. During ordinary glass formation, the atomic diffusion slows down, rendering its experimental investigation impractically long, to the extent that a timescale divergence is taken for granted by many. We circumvent these limitations here, taking advantage of a wide family of glasses rapidly obtained by physical vapor deposition directly into the solid state, endowed with different "ages" rivaling those reached by standard cooling and waiting for millennia. Isothermally probing the mechanical response of each of these glasses, we infer a correspondence with viscosity along the equilibrium line, up to exapoise values. We find a dependence of the elastic modulus on the glass age, which, traced back to the temperature steepness index of the viscosity, tears down one of the cornerstones of several glass transition theories: the dynamical divergence. Critically, our results suggest that the conventional wisdom picture of a glass ceasing to flow at finite temperature could be wrong.

glass transition | supercooled liquid | aging | vibrational properties | inelastic scattering

A wide range of liquids can be cooled below the freezing point avoiding crystallization. Under such circumstances, viscosity increases dramatically, up to the point where the system falls out of equilibrium (1–4). Whether (5–10) or not (11–16) this increase signals a divergent behavior is a question hitting at the core of any glass transition theory, and has attracted an increasing number of experimental investigations (17–27).

The thermal history of a liquid engraves the properties of the resulting, amorphous material (glass), which continuously hikes down a rugged energy landscape to enhance its stability in search of lower minima (28, 29). From an opposite perspective, the way the equilibrium properties of a unique liquid are encoded in the peculiarities of different corresponding glasses, each endowed with different histories and stabilities, has always puzzled scientists and technologists (3, 30). The fictive temperature T_f, for instance, unambiguously signals the out-of-equilibrium arrested state accompanying the glass transition (31), and increases with the cooling speed, which is upper limited by the finite thermal conductivity of the sample. Upon slowing down the quenching rate, the system gets trapped in lower potential energy landscape basins (inherent structures), but crystallization is also facilitated. In an attempt to rationalize such phenomenology, one way to define the glass transition temperature is the fictive temperature at a conventional cooling rate: $T_g = T_f(-10\ \mathrm{K/min})$. Correspondingly, the system falls out of equilibrium over a timescale of ≈ 100 s, attaining viscosities of 10^{11}–10^{13} poise. The impact of such an arbitrariness is mitigated by the observation that for bulk materials, ordinary cooling rates are often confined in the range −0.1 to −10 K/min and T_f varies very little. Remarkably, this severely limits the free-energy region accessible by the glass, at least on timescales useful for many potential applications. It has been recently shown (28, 32–34), however, that the limitations in exploring the bottom of the energy landscape can be circumvented synthesizing glasses directly well below T_g, avoiding the supercooling route by physical vapor deposition (PVD). These glasses are referred to as ultrastable, for their enhanced resistance against crystallization, and populate free-energy regions as low as those of semifossilized resins (17) aged for thousands of years.

Indomethacin (IMC), selected for this study, is a prototype organic glass-former endowed with antipyretic properties, which, in its crystalline form, has poor water solubility and bioavailability (35), limitations partially removed in the amorphous phase. Obtaining ultrastable amorphous IMC on laboratory timescales does not improve water solubility, but enables a unique opportunity to approach the so-called "ideal glass," i.e., an amorphous phase with the same entropy of the underlying crystalline form.

Results

Glass stability can be quantified by determining T_f from the endothermic jump exhibited by the specific heat upon fast heating (36), due to the transformation of the glass into supercooled liquid (*Materials and Methods*). We present in Fig. 1 an assessment of the stabilities of IMC glasses prepared by PVD at six different substrate temperatures T_{sub} in the range 190–290 K, as determined using differential scanning calorimetry (DSC).

The T_fs of the depositions testify to their stability enhancement (compared with conventional glasses), which increases with the substrate temperature up to a maximum gap of 34 K with respect to T_g, achieved for the most ultrastable, i.e., lowest T_f case ($T_{sub} = 266$ K, in agreement with ref. 33). The reason for such stability enhancement, attained by tuning T_{sub}, has been traced back to the increase of the surface mobility, which is believed to allow molecules to arrange themselves into lower energy

Significance

"Does the glass cease to flow at some finite temperature?" Answering this question—of pivotal importance for glass formation theories—would require ridiculously long observation times. We circumvent this infeasibility relating the (directly inaccessible) ultraviscous flow of a liquid to the elastic properties of the corresponding glass, which we measure as a function of its age. The older the glass, the lower the temperature at which viscosity can be determined. Taking advantage of physical vapor deposition, we rapidly obtain a wide spectrum of ages rivaling those of millenary ambers, enabling viscosity determinations at values as large as those pertaining to the asthenosphere. Our result ultimately rules out the finite-temperature divergence of the molecular diffusion timescale in a glass.

Author contributions: T.S. conceived and supervised the research; C.R.-T. and J.R.-V. prepared the samples and carried on the calorimetric characterization; E.A.A.P. lead the Picosecond Photo-Acoustics measurements and data analysis, with contributions from G.C., C.F., and T.S.; and E.A.A.P. and T.S. wrote the paper.

The authors declare no conflict of interest.

This article is a PNAS Direct Submission.

[1]To whom correspondence should be addressed. Email: tullio.scopigno@phys.uniroma1.it.

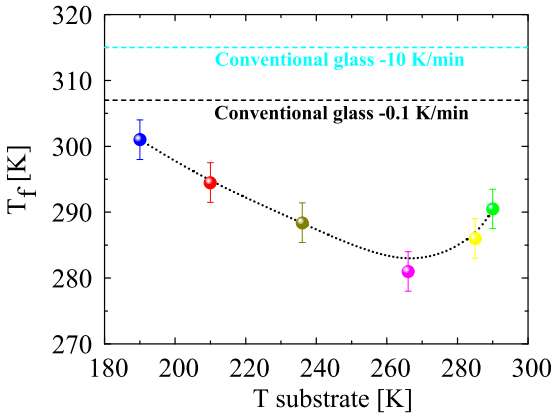

Fig. 1. Fictive temperature of PVD glasses as function of the substrate temperature during deposition, determined from DSC upscans, directly relates to the enthalpy content, hence quantifying the glass stability (see *Materials and Methods* for more details). Typical values obtained for conventional glasses for two different cooling rates are also indicated (dashed lines).

configurations (28, 32, 33). Specifically, for a given deposition rate, coming from the high-temperature side, the (relatively large) surface mobility grants that the glass is "assembled" in equilibrium with its liquid, i.e., each layer of molecules is equilibrated before new molecules arrive in the deposition process. Within this regime, the lower the temperature, the lower the entropy of the system and the higher the stability. Below a given temperature the mobility is so slow that the structure is no longer in equilibrium with the liquid, and the system becomes increasingly unstable.

Because the shape of the inherent structures of the energy landscape defines the vibrational properties, a question arises on the possible connection between mechanical response and glass stability, in connection with recent experimental evidence in amorphous depositions and naturally aged glasses (17, 37, 38). Specifically, previous studies (39) of IMC obtained by PVD reveal a sound velocity dependence on local substrate temperature which, in turn, has been shown to relate to the onset temperature of enthalpy release measured in calorimetry upscans (40). To address this issue we first studied the acoustic properties of the most ultrastable deposition by a combination of time-domain pump–probe optical spectroscopy and frequency-domain inelastic X-ray scattering (IXS). The former technique is a broadband version (41, 42) of picosecond photoacoustics (BPA) (43), which we recently developed to efficiently generate and detect longitudinal acoustic wavepackets in sub-μm-thick transparent layers. Specifically, by using white light pulses (450–650 nm), the energy dispersion and mode attenuation of the vibrational excitations have been simultaneously investigated in the frequency range 10–20 GHz. IXS, on the other hand, allows the study of the high-frequency limit (THz), where the characteristic excitation wavelengths approach the average interparticle distance and the structural disorder becomes of crucial importance. Further details on both the techniques are given in *Materials and Methods*. The dispersion curve as determined by BPA in the low-frequency regime, and by IXS in the mesoscopic regime, is reported in Fig. 2, along with the photoinduced differential reflectivity oscillations map and IXS spectra at fixed exchanged momenta (Fig. 2, *Insets A* and *B*), from which the dispersion is obtained.

In the low-frequency region, the linear energy dispersion indicates the existence of propagating vibrational excitations corresponding to a single longitudinal acoustic-like phonon branch. Remarkably, the propagating nature of these excitations lingers up to the THz frequency regime. The presence of structural disorder, indeed, strongly attenuates acoustic modes at the nanometer scale. Nevertheless, the existence of a well-defined first sharp diffraction peak mimics a first pseudo-Brillouin zone and, although the vibrational eigenmodes are no longer plane waves, a well-defined dominant wavevector still exists up to a zero-group velocity point corresponding to half of the pseudo-Brillouin zone boundary (44). The obtained sound velocity (the $q=0$ derivative of the best sinusoidal fit to IXS data, dashed line in Fig. 2) is in excellent agreement with BPA data in the 10-GHz range and with previous single- (lower) frequency determination (37). The existence of a well-defined dispersion at any lengthscales within

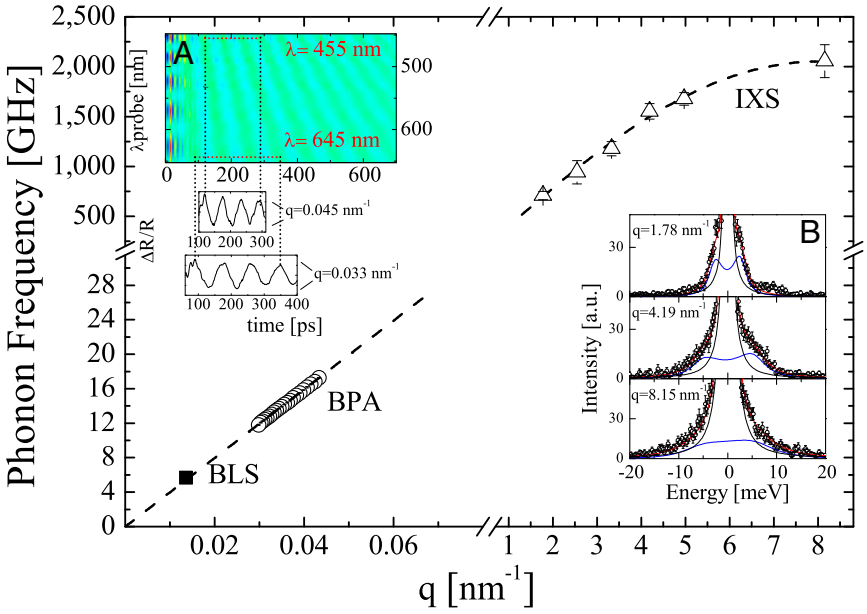

Fig. 2. Longitudinal acoustic phonon dispersion in ultrastable PVD glass (T_{sub} = 266 K), investigated by IXS (△, dashed line is the sinusoidal best fit) in the THz regime, by BPA (○) in the GHz regime, along with a previous Brillouin measurement (□) at lower frequency (37). (*A*) Transient reflectivity BPA data; each λ_{probe} couples to a phonon of well-defined wavevector, visualized as an oscillatory signal in time domain. (*B*) IXS spectra, acoustic phonons for selected wavevectors, *Q*, probed in frequency domain.

a pseudo-Brillouin zone suggests the potential sensitivity of the acoustic properties to the local topology of the inherent structures visited by the glass. Given their capability to access a sizable portion of the dispersion curve, determining sound velocity with superior accuracy (down to 0.1%, about one order of magnitude better than ordinary Brillouin light scattering), BPA measurements have been extended to the other PVD samples as shown in Fig. 3 *A* and *B*. During the experiments the temperature was kept constant at $T = 295$ K, i.e., well below T_g and above the T_f of the different depositions, to ensure that the glass state is arrested on the laboratory timescale.

A clear inverse correlation between sound velocity and T_f arises. BPA experiments also enable determination of the hypersonic attenuation Γ with an accuracy of tenths of GHz, and, accordingly, determination of the frequency dependence of the lifetime of the vibrational excitations. As an example, the frequency dependence of Γ for $T_f = 281$ and 301 K is reported (pink and blue, respectively) in Fig. 3*C*. Aiming to unravel any link with T_f, we integrated the attenuation over the explored frequency range and calculated the excess relative (and normalized) to the most ultrastable glass ($T_f = 281$ K), as reported in Fig. 3*D*. The relative attenuation shows, similarly to the sound velocity, a clear but opposite (direct) correlation with T_f. Acoustic attenuation in disordered materials is ruled by different physical mechanisms (42). In the GHz regime, where a crystal-like picture of vibrational excitations holds, the attenuation is expected to be due to the anharmonicity of the interparticle interaction. The decrease of sound attenuation toward the lowest T_fs discussed above, therefore, corroborates the idea that lower energy basins are more harmonic in nature.

Discussion

The distinct thermomechanical correlation reported in this study has important implications for the validity of those paradigms which can be uniquely benchmarked at the liquid side of the glass transition, because equilibration times dramatically increase below T_g preventing direct explorations. Fragility, in particular, quantifies the steepness of the liquid viscosity (or equivalently the relaxation time, through Maxwell's relation $\eta = G_\infty \tau$) at T_g, and it has a pivotal role in controlling physical properties of the supercooled phase (2, 3). The provocative idea that fast degrees of freedom characterizing glass dynamics well below T_g can be predictors for slow dynamical properties of the liquid state, such as the structural relaxation time and hence fragility, is rapidly gaining consensus (4, 45–48). Whereas density fluctuations completely decorrelate in a liquid, as a consequence of the ergodic sampling of different basins in the energy landscape, in a glass a residual correlation exists, uniquely determined by the entire spectrum of vibrational eigenstates of the energy minimum where the system is trapped. This is the so-called nonergodicity factor (NEF), the long-time limit of the density–density autocorrelation function. Of interest here, it has been shown that the liquid fragility m can be determined by the low-temperature behavior of the NEF, $f_q(T)$ (46, 47). The NEF can be quantified in different ways among them by the relative sound velocity jump occurring at the glass transition (49, 50), namely,

$$m = \gamma \cdot \left(f^{-1}(T_g) - 1\right) \approx 140 \frac{c_0^2}{c_\infty^2 - c_0^2}, \qquad [1]$$

where c_0 and c_∞ are the liquid and glass sound velocity values, respectively, and $\gamma \approx 140$ expresses the above-discussed correlation with fragility m (46), verified in ordinary IMC glass (51). Critically, c_0 is an equilibrium property of the liquid, whereas c_∞ is shown here to depend upon the very stability of the corresponding glass. This advocates the extension of the fragility concept to a temperature-dependent steepness index (11) $I(T)$ such that $I(T_g) = m$, which we use here to obtain the equilibrium viscosity below T_g. The mechanical response of a glass of a given stability, indeed, determines the viscosity of its liquid at the corresponding T_f, via the dependence $I(T = T_f) = I(c_\infty(T_f))$ in Eq. **1**, reported in Fig. 4*A*.

Integrating this latter (see Eq. **11** in *Materials and Methods*), an Arrhenius plot can ultimately be obtained, shown in Fig. 4*B*. The super-Arrhenius behavior documented in IMC above T_g (52) is reported as a dashed line representing a Vogel–Fulcher–Tamman (VFT) function. For $T < T_g$ a remarkable deviation is observed: The apparent fragility $I(T)$ is larger than m, but falls below the VFT expectation, and decreases with the glass stability, signifying a fragile-to-strong transition, quantified in Fig. 4*A*. This result verifies the predictions of Kovacs and Adam–Gibbs–Vogel models from aged IMC (27) and rationalizes very recent work in naturally long-time–aged amber (17), which set an upper bound to the temperature dependence of the dynamics below T_g. It is also in line with the conclusion against the VFT extrapolations in the glass (11, 53), and relates to the observation of an additional non-Arrhenius equilibration process in polymers (54). Moreover, the simultaneous decrease of both the acoustic attenuation and generalized fragility reported here at low T_fs validates recent molecular dynamic simulations (55) which put forward a direct correlation between kinetic fragility m and the degree of anharmonicity of the interparticle interaction potential.

All together, these evidences syncretize on the scenario schematically depicted in Fig. 4, establishing a firm link between the hypsometric characterization of the energy landscape and basin-specific vibrational properties. Crucial to technological applications, the mechanical approach advanced here to assess stability is a nondestructive one, as opposed to calometric determinations of T_f. Most important, we demonstrate that the state of the glass is totally identified by T_f and T, and once the nonergodicity parameter is calculated by the sound velocity jump at T_f it is possible to determine the relaxation time from Eqs. **1** and **11**, as shown in Fig. 4. The emerging protocol provides

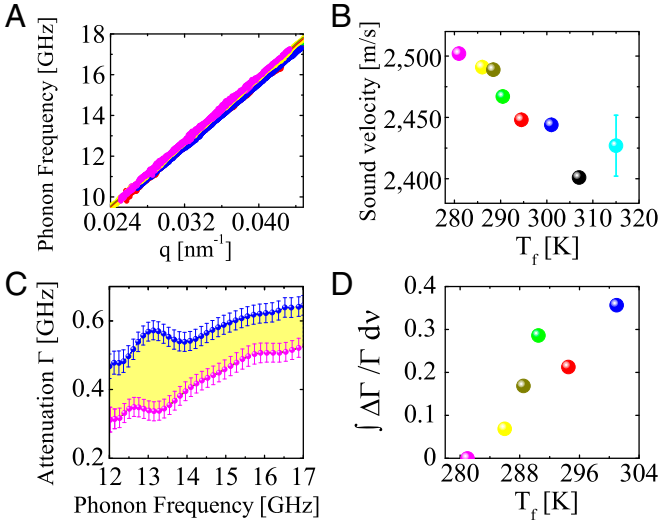

Fig. 3. Sound velocity and damping for different stabilities. (*A*) GHz-dispersion curves of the longitudinal acoustic phonons from isothermal BPA measurements ($T = 295$ K). (*B*) Sound velocity (linear fit to the dispersion curves) exhibits a correlation with T_f, showing a maximum for $T_f = 281$ K. Error bars smaller than the symbol. The values for conventional glasses ($T_f = 307$ K and $T_f = 315$ K) are from refs. 37 and 51, respectively. (*C*) Acoustic attenuation Γ for depositions with high ($T_f = 281$ K, pink) and low ($T_f = 301$ K, blue) stabilities as function of the phonon frequency. (*D*) Normalized excess acoustic attenuation relative to the most ultrastable glass, obtained integrating over the explored frequency range and normalizing to the $T_f = 281$ K case. An inverse correlation respect to that in sound velocity is observed.

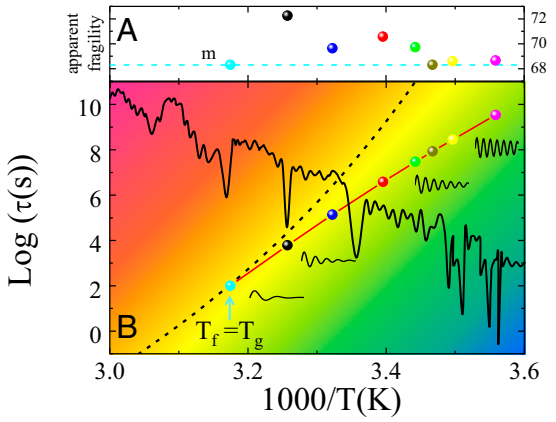

Fig. 4. Viscous flow of a liquid and stability of its glasses. (*A*) Apparent fragility $I(T)$, determined from the sound velocity jump in glasses with different T_f, indicates a fragile to strong transition below T_g. Conventional fragility $m = I(T_g)$ is also reported. (*B*) Arrhenius plot for $T < T_g$, obtained integrating data from *A*. A correlation is found between the depth of the inherent structures in the energy landscape (gray line) probed by glasses of different T_f and the mechanical response (sketched by time-domain damped oscillations). The VFT behavior obtained from above T_g data (52) is also shown (dashed line).

a unique way to capture essential features of a liquid attaining the structural arrest away from T_g, up to relaxation times beyond 10^9 s, corresponding to exapoise viscosities. In conclusion, we circumvented here the major hindrances to probe equilibrium properties below the ordinary glass transition temperature: crystallization tendency and unrealistic observation times. The isothermal measurement of mechanical properties for glassy phases with different T_f reveals the increase of the longitudinal elastic modulus and decrease of the acoustic loss below T_g, which we connect to a breakdown of the VFT law. This may lead to reconsideration of old paradigms based on the dynamical divergence to ever reach a definitive understanding of the glass transition.

Materials and Methods

Sample Growth and Thermal Characterization and Treatment. IMC [99% purity, T_g= 315 K, and T_m (γ-form) = 428 K] crystalline powders were purchased from Sigma-Aldrich. Twin films of ultrastable IMC glasses were grown by vapor deposition on Si (100) substrates and on DSC Al pans at deposition temperatures spanning from 190 to 290 K. An effusion cell filled with IMC was heated to achieve the desired deposition rate of 0.1 nm/s, as measured by a quartz crystal microbalance. When this rate was attained, the shutter was removed to start deposition. The thickness of the films ranges from 1.5 to 2 μm, for the BPA experiments, to 50 μm for the IXS measurements. All samples were stored in vacuum-sealed bags with desiccant in the freezer to minimize aging before the acoustic measurements, which were carried out several days after the deposition. DSC was performed immediately after removing the samples from the growth chamber (56). A DSC Perkin-Elmer 7 was used to monitor the power absorbed–released during heating scans at a rate of 10 K/min on IMC films of 2–10 mg. The first scan typically corresponds to an ultrastable glass, whereas the second one is characteristic of a glass obtained by cooling the liquid at −10 K/min. The fictive temperature is measured, evaluating the intersection of the enthalpy curves of the PVD glasses, i.e., the integral of the heat capacity upscans, with the supercooled liquid line extrapolated according to a quadratic fit (32). Notably, the extrapolated value of the fictive temperature does not depend on the heating rate and directly reflects the structural state of the glass. The lower values of the fictive temperature of ultrastable glasses signify a smaller enthalpy content compared with the glasses cooled at ordinary rates.

IXS. The IXS experiments were performed at the beam line ID28 of the European Synchrotron Radiation Facility. The experimental observable is the frequency spectrum of the scattered X-ray intensity, proportional to the dynamic structure factor $S(q,\hbar\omega)$, where q is the exchanged momentum defined by the scattering angle θ and by the wavevector of the incident photons k_i as $q = 2k_i \sin(\theta/2)$. An 8-analyzers bench was used, operating in horizontal scattering geometry. The sample was mounted with the substrate parallel to the scattering plane, tightly focusing the beam down to 20 μm in the vertical direction to avoid parasitic scattering from the substrate. With such a geometry the probed phonon direction is orthogonal to the growth. Energy scans were performed at constant q values in the range 1–8 $\approx$ nm^{-1}, corresponding to half of the pseudo-Brillouin zone (q = 14.7 nm^{-1}). The q resolution, determined by slits placed in front of the analyzer, was set to 0.25 nm^{-1}. The scanned energy range was $-30 \le \hbar\omega \le 30$ meV, where $\hbar\omega = E_0 - E$ is the energy transfer, with E_0 and E being the energy of the incident (23.725 eV) and the scattered X-ray photon, respectively; each scan took ~480 min. Using the (12, 12, 12) reflection for the Si monochromator and crystal analyzers the overall energy resolution was 1.5 meV, determined as the FWHM of instrumental response function (black line under the spectra in Fig. 2). Measurements were performed at room temperature (T = 295 K) on a sample grown by PVD at substrate temperature T_{sub} = 266 K and deposition rate of 0.1 nm/s, 50 μm thick. The dynamic structure factor, $S(q,\hbar\omega)$, contains information about the sound dispersion $\Omega(q)$ and attenuation $\Gamma(q)$ which can be extracted by a damped harmonic oscillator model:

$$S(q,\omega) = S(q)\left[\delta(\omega)f_q + \frac{(1-f_q)}{\pi}\frac{\Omega(q)^2\Gamma(q)}{\left[\omega^2-\Omega(q)^2\right]^2+\omega^2\Gamma^2(q)}\right]\cdot\frac{\hbar\omega/(k_BT)}{1-e^{\hbar\omega/(k_BT)}}, \quad [2]$$

where the Bose factor accounts for the quantum nature of the probed excitations. The two terms in Eq. **2** represent the elastic and the inelastic components of the spectra, respectively. Eq. **2** was fitted to the experimental data after a correction for the finite instrument resolution (57). The IXS sound velocity measurement of the ordinary glass reported in Fig. 3*B* accounts for a 0.8% positive dispersion occurring in the THz regime (51, 58).

Picosecond Photoacoustics. Time-domain measurements of longitudinal sound velocity and acoustic damping in the hydrodynamics limit were performed by broadband picosecond photoacoustics. This pump-and-probe technique is based on the generation and detection of coherent vibrational excitations by means of ultrashort laser pulses. The setup is built on a regeneratively amplified Ti:sapphire laser producing 50-fs, 4-mJ pulses at 800 nm with 1-kHz repetition rate. The output is split to generate both the pump and the probe beams; the former, after passing through a delay line, is focused onto the sample on an $\approx$ 100-μm spot diameter with energies up to 5 μJ. The PVD glasses of IMC, 1.5–2 μm thick, have been deposited onto a crystalline Si substrate at six different substrate temperatures (T_{sub} = 190, 210, 236, 266, 285, and 290 K) and coated by a 15-nm-thick layer of Ni. As the pump impinges on the sample, it is partially absorbed by the metallic coating, which thermally expands, launching in the underlying glass very short strain pulses, i.e., longitudinal acoustic wavepackets with a characteristic spectrum extending from a few to hundreds of GHz (43). The photogenerated acoustic wavepacket travels inside the sample along the growth direction. A portion of the probe pulse is reflected at the metallic surface, whereas the transmitted component interferes with the light scattered from the traveling density fluctuation associated with the acoustic wavepacket. By monitoring transient differential reflectivity (with and without the pump pulse) $(\Delta R(t))/R$ as a function of the time pump–probe time delay, information can be gained on the phonon spectrum. Specifically, at any given probe wavelength λ, the phonon frequency is set by the Bragg condition corresponding to a stimulated Brillouin scattering event:

$$\nu = \frac{v}{2\pi}q = \frac{2v_s}{\lambda}\sqrt{n^2-\sin^2\beta}, \quad [3]$$

where v is the longitudinal sound velocity, q the exchanged momentum, $n(\lambda)$ the index of refraction of the glass, and β is the incident angle with respect to the metallic coating. In our realization, the probe pulse consisted of a broadband white light continuum, generated from 2-mm-thick sapphire crystal plate and filtered to select wavelengths in the range 450–650 nm. The broadband probe pulse's reflection was dispersed by a 150-g/mm grating and monitored by a CCD, such that a number of two-color pump-and-probe experiments were simultaneously recorded. Transient reflectivity data were first reduced by subtraction of an exponential thermal background. Each channel achieves a sensitivity up to $\Delta R/R \approx 10^{-5}$. To get rid of an independent determination of the refractive index n, required in Eq. **3**, the measurements were repeated at different scattering angles β. A selection of the reflectivity oscillations as a function of time and probe wavelength is reported in the color map in Fig. 2 together with the signals at selected wavelengths. The signal was modeled with the damped harmonic oscillator

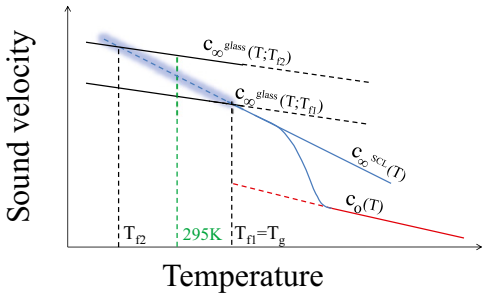

Fig. 5. Temperature dependence of the sound velocity for two glasses of different fictive temperature T_f, along with the unique liquid and supercooled liquid values. The shaded line indicates the region of the highly viscous supercooled liquid, where direct observations are prevented by impractically long equilibration timescales.

in the time domain, whose frequency can be estimated with an accuracy of 0.1%. The sound velocity was determined from the linear fit of the modes' frequency ν as a function of the exchanged momentum q over all of the broadband probed range. The acoustic attenuation, indeed, was directly extracted from the damping of the reflectivity oscillations with 6% accuracy.

Temperature Dependence of the Relaxation Time. The so-called kinetic fragility quantifies the temperature behavior of the relaxation time $\tau(T)$ at a conventional fictive temperature (T_g) where $\tau = 100$ s. Namely,

$$m = \left.\frac{\partial \log_{10}\tau}{\partial(T_g/T)}\right|_{T=T_g}. \quad [4]$$

To describe the low-temperature dependence of the NEF $f_q(T)$ in the low-q limit, a dimensionless steepness index can be introduced:

$$\alpha = -\lim_{q\to 0}\left.\frac{\partial f}{\partial \frac{T}{T_g}}\right|_{T=0}. \quad [5]$$

Remarkably, α exhibits a strong direct correlation with the kinetic fragility m, as it has been demonstrated experimentally (46, 47, 59, 60) and by numerical simulations (55) for a sizable number of glass-formers. Accordingly, the faster the T dependence of $f_q(T)$, i.e., the higher the value of α, the more fragile the glass-former. Below fragilities as high as 100, the correlation is linear:

$$m = \gamma\alpha, \quad [6]$$

with $\gamma \approx 140$. In the harmonic approximation, the T dependence of $f_q(T)$ reads

$$f_q(T) = \frac{1}{1+\alpha\frac{T}{T_g}}. \quad [7]$$

The value of $f_q(T_g)$ can be conveniently determined from the glass (c_∞) → liquid (c_0) sound velocity jump around the glass transition, through the expression

$$f_q(T_g) = 1 - \left.\frac{c_0^2}{c_\infty^2}\right|_{T_g}. \quad [8]$$

By evaluating Eq. **7** at $T = T_g$, and combining it with Eq. **8**, it immediately follows:

$$m = \gamma\left.\frac{c_0^2}{c_\infty^2 - c_0^2}\right|_{T_g}. \quad [9]$$

Besides the measurement temperature, however, the glass velocity also depends upon stability, i.e., on the fictive temperature T_f. This can be taken into account by generalizing Eq. **9** as

$$\left.\frac{\partial \log_{10}\tau}{\partial(T_f/T)}\right|_{T=T_f} = \gamma\left.\frac{c_0^2(T)}{c_\infty^2(T_f,T) - c_0^2(T)}\right|_{T=T_f} = I(T_f), \quad [10]$$

where the notation $c_\infty(T_f,T)$ explicitly indicates the above-mentioned dependencies on fictive and measurement temperatures, respectively. It is worth mentioning that the T dependence in Eq. **10** (i.e., on the very temperature where the sound velocity jump is evaluated) is negligible compared with the T_f dependence brought about by the glass sound velocity. Once integrated in $1/T$, Eq. **10** provides the relaxation time below T_g through

$$\log_{10}\tau(1/T_f) = \log_{10}\tau(1/T_g) + T_f\int_{T_g^{-1}}^{T_f^{-1}} I(T')d(1/T'), \quad [11]$$

with $c_0(T_g) = 1{,}354$ m/s estimated by Brillouin light scattering (61), and the $c(T)$ dependence is from ref. 37. In Fig. 5 we sketch the evolution of the sound velocity as function of temperature across the glass transition, for two glasses of different fictive temperature.

ACKNOWLEDGMENTS. We thank M. I. Alonso and M. Garriga from Institut de Ciència de Materials de Barcelona for the ellipsometric measurements, and the ID28 staff for the support during the IXS experiment. T.S. acknowledges enlightening discussions with C. A. Angell, S. Capaccioli, D. Cangialosi, J. Dyre, K. Ngai, S. Sastry, and F. Sciortino. E.A.A.P., C.F., and T.S. have received funding from the European Research Council (ERC) under the European Community's Seventh Framework Program (FP7/2007-2013)/ERC Grant Agreement 207916. C.R.-T. and J.R.-V. acknowledge financial support from Generalitat de Catalunya and Ministerio de Economa y Competitividad through Grants SGR2009-01225 and MAT2013-40896-P, respectively. G.C. acknowledges support by the European Community under Graphene Flagship (Contract no. CNECT-ICT-604391).

1. Angell CA, Ngai KL, McKenna GB, McMillan PF, Martin SW (2000) Relaxation in glassforming liquids and amorphous solids. *J Appl Phys* 88(6):3113–3157.
2. Angell CA (1995) Formation of glasses from liquids and biopolymers. *Science* 267(5206): 1924–1935.
3. Greer AL, Kelton KF, Sastry S, eds (2014) *Fragility Of Glass-forming Liquids, Texts and Readings in the Physical Science-13* (Hindustan Book Agency, Bengaluru, India).
4. Ngai KL (2000) Dynamic and thermodynamic properties of glass-forming substances. *J Non-Cryst Solids* 275(1-2):7–51.
5. Lubchenko V, Wolynes PG (2007) Theory of structural glasses and supercooled liquids. *Annu Rev Phys Chem* 58:235–266.
6. Wisitsorasak A, Wolynes PG (2014) Dynamical heterogeneity of the glassy state. *J Phys Chem B* 118(28):7835–7847.
7. Dudowicz J, Freed KF, Douglas JF (2007) Generalized entropy theory of polymer glass formation. *Advances in Chemical Physics*, ed Rice SA (John Wiley and Sons, Inc., Hoboken, NJ), Vol 137, pp 125–222.
8. Richert R (2013) Comment on "Temperature divergence of the dynamics of a poly (vinyl acetate) glass: Dielectric vs. mechanical behaviors" [J Chem Phys 136:154901 (2012)]. *J Chem Phys* 139(13):137101.
9. Wagner H, Richert R (1997) Thermally stimulated modulus relaxation in polymers: Method and interpretation. *Polymer (Guildf)* 38(23):5801–5806.
10. Richert R, Wagner H (1998) The dielectric modulus: Relaxation versus retardation. *Solid State Ion* 105(14):167–173.
11. Hecksher T, Nielsen AI, Olsen NB, Dyre JC (2008) Little evidence for dynamic divergences in ultraviscous molecular liquids. *Nat Phys* 4:738–741.
12. Di Marzio EA, Yang AJM (1997) Configurational entropy approach to the kinetics of glasses. *J Res Natl Inst Stand Technol* 102(2):135–157.
13. Wojnarowska Z, Ngai KL, Paluch M (2014) Deducting the temperature dependence of the structural relaxation time in equilibrium far below the nominal Tg by aging the decoupled conductivity relaxation to equilibrium. *J Chem Phys* 140(17): 174502.
14. Ngai KL, Capaccioli S, Paluch M, Prevosto D (2014) Temperature dependence of the structural relaxation time in equilibrium below the nominal T(g): Results from free-standing polymer films. *J Phys Chem B* 118(20):5608–5614.
15. Elmatad YS, Chandler D, Garrahan JP (2009) Corresponding states of structural glass formers. *J Phys Chem B* 113(16):5563–5567.
16. Elmatad YS, Chandler D, Garrahan JP (2010) Corresponding states of structural glass formers. II. *J Phys Chem B* 114(51):17113–17119.
17. Zhao J, Simon SL, McKenna GB (2013) Using 20-million-year-old amber to test the super-Arrhenius behaviour of glass-forming systems. *Nat Commun* 4:1783.
18. OConnell PA, McKenna GB (1999) Arrhenius-type temperature dependence of the segmental relaxation below tg. *J Phys Chem B* 110(22):11054–11060.
19. McKenna GB, Zhao J (2015) Accumulating evidence for non-diverging time-scales in glass-forming fluids. *J Non-Cryst Solids* 407:3–13.
20. Zhao J, McKenna GB (2012) Temperature divergence of the dynamics of a poly(vinyl acetate) glass: Dielectric vs. mechanical behaviors. *J Chem Phys* 136(15):154901–154908.
21. Zhao J, McKenna GB (2013) Response to "Comment on 'Temperature divergence of the dynamics of a poly(vinyl acetate) glass: Dielectric vs. mechanical behaviors'" [J Chem Phys 139:137101 (2013)]. *J Chem Phys* 139(13):137102.
22. Simon SL, Sobieski JW, Plazek D (2001) Volume and enthalpy recovery of polystyrene. *Polymer (Guildf)* 42:2555–2567.
23. Badrinarayanan P, Simon SL (2007) Origin of the divergence of the timescales for volume and enthalpy recovery. *Polymer (Guildf)* 48:1464–1470.

24. Koh YP, Simon SL (2013) Enthalpy recovery of polystyrene: Does a long-term aging plateau exist? *Macromolecules* 46(14):5815–5821.
25. Simon SL, Plazek DJ, Sobieski JW, McGregor ET (1997) Physical aging of a polyetherimide: Volume recovery and its comparison to creep and enthalpy measurements. *J Polym Sci, Part B: Polym Phys* 35(6):929–936.
26. Echeverra I, Kolek PL, Plazek DJ, Simon SL (2003) Enthalpy recovery, creep and creep recovery measurements during physical aging of amorphous selenium. *J Non-Cryst Solids* 324(3):242–255.
27. Brian CW, Zhu L, Yu L (2014) Effect of bulk aging on surface diffusion of glasses. *J Chem Phys* 140(5):054509.
28. Parisi G, Sciortino F (2013) Structural glasses: Flying to the bottom. *Nat Mater* 12(2): 94–95.
29. Sastry S (2001) The relationship between fragility, configurational entropy and the potential energy landscape of glass-forming liquids. *Nature* 409(6817):164–167.
30. Chang K (July 29, 2008) The nature of glass remains anything but clear. *NY Times*, Section Science. Available at www.nytimes.com/2008/07/29/science/29glass.html?pagewanted=all&_r=0#. Accessed February 2, 2015.
31. Tool AQ (1946) Relation between inelastic deformability and thermal expansion of glass in its annealing range. *J Am Ceram Soc* 29:240–253.
32. Kearns KL, et al. (2008) Hiking down the energy landscape: Progress toward the Kauzmann temperature via vapor deposition. *J Phys Chem B* 112(16):4934–4942.
33. Swallen SF, et al. (2007) Organic glasses with exceptional thermodynamic and kinetic stability. *Science* 315(5810):353–356.
34. Leon-Gutierrez E, Sepúlveda A, Garcia G, Clavaguera-Mora MT, Rodríguez-Viejo J (2010) Stability of thin film glasses of toluene and ethylbenzene formed by vapor deposition: An in situ nanocalorimetric study. *Phys Chem Chem Phys* 12(44): 14693–14698.
35. Hancock BC, Zografi G (1997) Characteristics and significance of the amorphous state in pharmaceutical systems. *J Pharm Sci* 86(1):1–12.
36. Moynihan CT, Easteal AJ, DeBolt MA (1976) Dependence of the fictive temperature of glass on cooling rate. *J Am Ceram Soc* 59(1-2):12–16.
37. Kearns KL, Still T, Fytas G, Ediger MD (2010) High-modulus organic glasses prepared by physical vapor deposition. *Adv Mater* 22(1):39–42.
38. Pérez-Castañeda T, Jiménez Riobóo RJ, Ramos MA (2013) Low-temperature thermal properties of a hyperaged geological glass. *J Phys Condens Matter* 25(29):295402.
39. Fakhraai Z, Still T, Fytas G, Ediger MD (2011) Structural variations of an organic glassformer vapor-deposited onto a temperature gradient stage. *J Phys Chem Lett* 2: 423–427.
40. Dalal SS, Fakhraai Z, Ediger MD (2013) High-throughput ellipsometric characterization of vapor-deposited indomethacin glasses. *J Phys Chem B* 117(49):15415–15425.
41. Pontecorvo E, et al. (2011) Visualizing coherent phonon propagation in the 100 GHz range: A broadband picosecond acoustics approach. *Appl Phys Lett* 98:011901.
42. Ferrante C, et al. (2013) Acoustic dynamics of network-forming glasses at mesoscopic wavelengths. *Nat Commun* 4:1793.
43. Thomsen C, Strait J, Vardeny Z, Maris HJ, Tauc J (1984) Coherent phonon generation and detection by picosecond light pulses. *Phys Rev Lett* 53(10):989–992.
44. Sette F, Krisch MH, Masciovecchio C, Ruocco G, Monaco G (1998) Dynamics of glasses and glass-forming liquids studied by inelastic x-ray scattering. *Science* 280(5369): 1550–1555.
45. Buchenau U, Zorn R (1992) A relation between fast and slow motions in glassy and liquid selenium. *Europhys Lett* 18(6):523–528.
46. Scopigno T, Ruocco G, Sette F, Monaco G (2003) Is the fragility of a liquid embedded in the properties of its glass? *Science* 302(5646):849–852.
47. Scopigno T, Cangialosi D, Ruocco G (2010) Universal relation between viscous flow and fast dynamics in glass-forming materials. *Phys Rev B* 81:100202.
48. Larini L, Ottochian A, De Michele C, Leporini D (2008) Universal scaling between structural relaxation and vibrational dynamics in glass-forming liquids and polymers. *Nat Phys* 4:42–45.
49. Niss K, et al. (2008) Glassy properties and viscous slowing down: An analysis of the correlation between nonergodicity factor and fragility. *J Chem Phys* 129(19):194513.
50. Buchenau U, Wischnewski A (2004) Fragility and compressibility at the glass transition. *Phys Rev B* 70:092201.
51. Pogna EAA, Rodríguez-Tinoco C, Krisch M, Rodríguez-Viejo J, Scopigno T (2013) Acoustic-like dynamics of amorphous drugs in the THz regime. *Sci Rep* 3:2518.
52. Carpentier L, Decressain R, Desprez S, Descamps M (2006) Dynamics of the amorphous and crystalline α-, γ-phases of indomethacin. *J Phys Chem B* 110(1):457–464.
53. Mauro JC, Yue Y, Ellison AJ, Gupta PK, Allan DC (2009) Viscosity of glass-forming liquids. *Proc Natl Acad Sci USA* 106(47):19780–19784.
54. Cangialosi D, Boucher VM, Alegría A, Colmenero J (2013) Direct evidence of two equilibration mechanisms in glassy polymers. *Phys Rev Lett* 111(9):095701.
55. Bordat P, Affouard F, Descamps M, Ngai KL (2004) Does the interaction potential determine both the fragility of a liquid and the vibrational properties of its glassy state? *Phys Rev Lett* 93(10):105502.
56. León-Gutierrez E, et al. (2008) In situ nanocalorimetry of thin glassy organic films. *J Chem Phys* 129(18):181101.
57. Scopigno T, Ruocco G, Sette F (2005) Microscopic dynamics in liquid metals: The experimental point of view. *Rev Mod Phys* 77:881–933.
58. Bryk T, et al. (2010) Collective excitations in supercritical fluids: Analytical and molecular dynamics study of "positive" and "negative" dispersion. *J Chem Phys* 133(2): 024502.
59. Greaves GN, Greer AL, Lakes RS, Rouxel T (2011) Poisson's ratio and modern materials. *Nat Mater* 10(11):823–837.
60. Mauro J, Allan D, Potuzak M (2009) Nonequilibrium viscosity of glass. *Phys Rev B* 80: 094204.
61. De Panfilis S, Pogna EAA, Virga A, Scopigno T (2014) Acoustic dynamics of supercooled indomethacin probed by Brillouin light scattering. *Phys Chem Chem Phys* 16(27): 14206–14211.